energies

MDPI

Article

Computational and Experimental Research on the Influence of Supplied Gas Fuel Mixture on High-Temperature Fuel Cell Performance Characteristics

Iliya Krastev Iliev [1,*], Antonina Andreevna Filimonova [2], Andrey Alexandrovich Chichirov [2], Natalia Dmitrievna Chichirova [2] and Plamen Ganchev Kangalov [3]

[1] Department of Heat, Hydraulics and Environmental Engineering, "Angel Kanchev" University of Ruse, 7017 Ruse, Bulgaria
[2] Department "Chemistry and Hydrogen Energy", Kazan State Power Engineering University, 420066 Kazan, Russia; aachichirova@mail.ru (A.A.F.); pinpin3@yandex.ru (A.A.C.); ndchichirova@mail.ru (N.D.C.)
[3] Department "Repair, Reliability, Mechanisms, Machines, Logistic and Chemical Technologies", University of Ruse, 7017 Ruse, Bulgaria; kangalov@uni-ruse.bg
* Correspondence: iki@uni-ruse.bg

Abstract: Currently, the process of creating industrial installations is associated with digital technologies and must involve the stage of developing digital models. It is also necessary to combine installations with different properties, functions, and operational principles into a single system. Some tasks require the use of predictive modeling and the creation of "digital twins". The main processes during the fuel cell modeling involve electrochemical transformations as well as the movement of heat and mass flows, including monitoring and control processes. Numerical methods are utilized in addressing various challenges related to fuel cells, such as electrochemical modeling, collector design, performance evaluation, electrode microstructure impact, thermal stress analysis, and the innovation of structural components and materials. A digital model of the membrane-electrode unit for a solid oxide fuel cell (SOFC) is presented in the article, incorporating factors like fluid dynamics, mass transfer, and electrochemical and thermal effects within the cell structure. The mathematical model encompasses equations for momentum, mass, mode, heat and charge transfer, and electrochemical and reforming reactions. Experimental data validates the model, with a computational mesh of 55 million cells ensuring numerical stability and simulation capability. Detailed insights on chemical flow distribution, temperature, current density, and more are unveiled. Through a numerical model, the influence of various fuel types on SOFC efficiency was explored, highlighting the promising performance of petrochemical production waste as a high-efficiency, low-reagent consumption fuel with a superior fuel utilization factor. The recommended voltage range is 0.6–0.7 V, with operating temperatures of 900–1300 K to reduce temperature stresses on the cell when using synthesis gas from petrochemical waste. The molar ratio of supplied air to fuel is 6.74 when operating on synthesis gas. With these parameters, the utilization rate of methane is 0.36, carbon monoxide CO is 0.4, and hydrogen is 0.43, respectively. The molar ratio of water to synthesis gas is 2.0. These results provide an opportunity to achieve electrical efficiency of the fuel cell of 49.8% and a thermal power of 54.6 W when using synthesis gas as fuel. It was demonstrated that a high-temperature fuel cell can provide consumers with heat and electricity using fuel from waste from petrochemical production.

Keywords: solid oxide fuel cell (SOFC); hydrogen energy; numerical simulation; ANSYS Fluent

Citation: Iliev, I.K.; Filimonova, A.A.; Chichirov, A.A.; Chichirova, N.D.; Kangalov, P.G. Computational and Experimental Research on the Influence of Supplied Gas Fuel Mixture on High-Temperature Fuel Cell Performance Characteristics. *Energies* **2024**, *17*, 2452. https://doi.org/10.3390/en17112452

Academic Editor: Antonino S. Aricò

Received: 7 April 2024
Revised: 16 May 2024
Accepted: 19 May 2024
Published: 21 May 2024

1. Introduction

The process of creating industrial installations requires a close connection with digital technologies and must involve the digital model's creation. At the same time, "digital production" is being developed. It involves an accurate and reliable simulation of an

energy equipment operating cycle in a virtual environment, based on reliable performance identification and the prediction of unknown parameters. This is a necessary stage in the creation, simulation, and predictive analysis of combined energy generation systems.

The solid oxide fuel cell (SOFC) represents an innovative energy technology that is both resource-efficient and promising [1]. However, carrying out experimental studies under various operating conditions is often impractical due to technical and economic constraints. It can be challenging to measure all flow characteristics, such as temperature, pressure, or flow velocity distribution within a cell using experimental approaches. Consequently, the numerical modeling of SOFCs provides a viable alternative [2–4]. The accurate modeling of SOFCs poses a significant challenge as it requires the simultaneous calculation of equations related to mass, momentum, energy, charge, electron transfer, and electrochemistry at the interfaces of liquid, solid, and porous media. To address this complexity, sophisticated numerical modeling tasks can be effectively tackled using commercial software packages [5,6].

Computational fluid dynamics (CFD) is known as one of the most powerful tools for calculating the performance of new apparatus and installations. CFD allows for the visualization of flow field characteristics, thereby avoiding expensive experiments. The scientific literature describes the numerous advantages of implementing CFD techniques, such as the rapid assessment of geometric changes compared to laboratory tests, reduction of scaling problems, ability to study phenomena occurring under extreme conditions, and analysis of the underlying cause rather than just the effects [7–13].

There are several studies that have been carried out using the additional ANSYS Fluent SOFC module [14–17]. In this module, the electrolyte is represented as a pair of imaginary walls, called the "electrolyte surface", through which the movement of ions and electrons is simulated. The SOFC module provides the user with a varied choice of fuel options and allows the simulation of electrochemical processes and polarization inside the cell. The use of an additional SOFC module is convenient because the electrochemical model is included in the built-in libraries and there is no need to develop a numerical code to take into account electrochemical effects. ANSYS Fluent is capable of solving mass, momentum, and energy equations along cells. Electrochemical processes and electrode microstructure cannot be directly modeled through ANSYS Fluent, requiring the development of custom functions.

Over the past few years, research attention has been focused on the design and optimization of manifolds to ensure uniform flow distribution at the inlet of the fuel and air passages. Uniform inlet flow distribution improves heat transfer and reduces pressure loss along the flow channels. This results in lower fuel consumption, less vibration and noise, and reduced corrosion caused by flow irregularities [18,19].

Electrode microstructure has a significant impact on SOFC performance since losses can be directly related to the morphological properties of the microstructure. Thermal stresses within the cell are caused by microstructural defects and a mismatch in the coefficient of thermal expansion between the microstructure of the anode and cathode [20].

Another challenge in designing and extending the service life of SOFCs is the study of thermal stress. This is caused by a mismatch in the coefficient of thermal expansion between different components. Thermal stress can cause SOFC thermomechanical failure. Operating the cell at high temperatures, along with startup and shutdown cycles, further increases the effects of thermal stress. The analysis of heat transfer within a cell is considered the most important task in the study of high-temperature SOFCs. As a result of the analysis, temperature distributions are obtained, with the help of which thermal stresses are calculated [21,22].

Assessing the morphological properties of porous electrodes is important when modeling SOFCs. Many physicochemical properties at the micro level are difficult to study experimentally. A reverse optimization goal can be set here. In this process, the unknown parameters of the model are calculated in such a way as to minimize the difference between the results of the direct formulation of the problem and real experimental data. COMSOL

Multiphysics is an effective software package for implementing inverse solutions due to its ability to perform microstructural analysis [23].

The introduction of new devices and installations requires the use of numerical modeling methods, and software packages help to quickly carry out research on new designs. In addition, innovative designs generally have unusual geometries that cannot be easily modeled using internal tools [24,25].

For new designs, it is recommended to conduct full stack simulations to study mass transfer and thermal stresses. In this case, calculations should be carried out both when operating in stationary and transient modes [26].

Thus, the problems solved by numerical methods include electrochemical process modeling, collector design, performance modeling, the influence of electrode microstructure, thermal stress analysis, and the development of new SOFC structural elements [27–30].

Most researchers make many assumptions when modeling the influence of various parameters on the flow process in a fuel cell. Electrochemical reactions are often ignored. There are few studies in the literature regarding the optimization of a variety of SOFC configurations and the consideration of all electrochemistry, heat transfer, and mass transfer in porous media simultaneously [31]. Such a complex problem must be solved numerically when developing the new technical solutions and design features of the fuel cell, as well as when hybridizing the process with other power units. It is also important to conduct experimental verification.

Most SOFC numerical modeling studies are aimed at finding ways to improve fuel cell performance. In [32], a 3D SOFC model with an active area of 16 cm^2 was developed to investigate various parameters affecting performance. It is found that SOFC performance improves with increasing operating pressure due to the partial pressure and diffusivity of the reactant gases, which leads to a decrease in mass transfer resistance. Operating temperature improves the performance of the fuel cell. Moreover, performance depends on fuel consumption and does not depend on oxygen consumption.

In one study [33], using the example of a three-dimensional model for an SOFC on an anode support, it was shown that significant temperature gradients exist along the length of the element. The maximum temperature value for cross-flow is in the area of the element outlet. The distribution of current density is uneven, and the maximum current density is located at the interfaces between channels, ribs, and electrodes. Maximum current density results in a large excess potential and heat source in the electrodes, which negatively affects the overall performance and life of the fuel cells.

In [28], a 3D model was developed to elucidate the internal thermal conditions and heat transfer mechanism of a 1 kW flat solid oxide fuel cell unit. It has been shown that the change in internal temperature depends on the airflow, the heating of the incoming gas through the gas manifolds, and the gas temperature entering each repeating unit.

Research [15] showed that increasing the porosity of the anode layers leads to an increase in cell performance (up to 15%), higher fuel content (up to 8%), and a more uniform distribution of fuel in the electrode.

In another study [34], a simulation of a single-cell SOFC battery of direct internal reforming was carried out, in which the effect of cell geometry on the rate of reforming reaction inside the fuel cell was studied.

There are several comprehensive reviews on the results of solid oxide fuel cell numerical modeling related to the topic of direct internal reforming [35], mathematical modeling of SOFC methods [36], and hybrid energy systems with SOFC [37].

When analyzing publication activity from 2021 to 2024, it was revealed that the interest of researchers modeling SOFCs is aimed at studying the operation of a fuel cell using various types of organic and inorganic fuels, biofuels, and various agricultural and industrial wastes [12,14,16,27,38,39].

Moreover, one urgent task is to predict the operating parameters of high-temperature SOFC based on the numerical modeling of electrochemical and heat and mass transfer

processes depending on the composition of the gas fuel mixture for its effective utilization with high-performance indicators.

2. Model Description

Digital modeling was carried out on a personal computer with an Intel Xeon Gold processor, 512 GB of RAM and a 1 TB SSD drive for more accurate and faster mathematical modeling.

The calculations were performed using the Ansys 2020 R2 software system designed for finite element analysis.

The geometric model of the stack is built in accordance with the specification. The model in this study is based on anode-supported SOFC developed by Ningbo SOFCMAN, China. Flows enter/exit the fuel cell stack through gas inlets/outlets (manifolds). Each fuel cell unit consists of an electrolyte and porous electrodes with a system of gas distribution channels and interconnections. Thus, for a 30-element cell, there are 900 repeating blocks.

Hydrogen, methane/hydrogen (CH_4 and H_2), and a mixture of methane, hydrogen, water, carbon monoxide, and carbon dioxide, which are a product of the conversion of oil refining waste, were modeled as fuel. Inlet conditions, namely, gas flow parameters, cell geometry properties, and specified settings for creating a 3D model, are presented in Tables 1 and 2.

Table 1. Characteristics of SOFC module parameters.

Name	Characteristics		
Relaxation coefficient	0.3		
Total system voltage	0.1–1.1 V		
Electrolyte thickness	1.5×10^{-5} m		
Electrolyte resistivity	0.3 Ohm·m		
Constant exchange current densities	Anode		5300 A/m^2
	Cathode		2300 A/m^2
Reference mole fraction values	H_2		0.5
	H_2O		0.5
	O_2		0.5
Mass flow per 1 cell	Anode		1.45×10^{-6} kg/s
	Cathode		2.83×10^{-5} kg/s
Temperature	Anode		998 K
	Cathode		998 K
Substances: hydrogen fuel	Anode	H_2	0.97 mol%
		H_2O	0.03 mol%
	Cathode	O_2	0.21 mol%
Substances: methane	Anode	CH_4	0.4 mol%
		H_2O	0.6 mol%
	Cathode	O_2	0.21 mol%
Substances: synthesis gas	Anode	CH_4	0.002 mol%
		H_2	0.594 mol%
		H_2O	0.206 mol%
		CO	0.163 mol%
		CO_2	0.035 mol%
	Cathode	O_2	0.21 mol%

A mesh with tetrahedral cells was created in the Ansys 2020 R2 Workbench software package (Figure 1). The number of cells was 55 million. The mesh quality was 0.94. The computational grid was constructed using mathematical equations of mass and charge conservation, matter transfer, heat transfer, and ion and electronic charge balance.

Table 2. Materials and geometry characteristics of the SOFC model.

Name	Material	Characteristics	Value
Anode	YSZ + NiO	Density	5900 kg/m^3
		Specific heat	410 J/(kg·K)
		Thermal conductivity	6.23 W/(m·K)
		Tortuosity	3
		Porosity	0.3
		Permeability	1×10^{-12}
		Electrical conductivity	333,330 S/m
		Length	100 mm
		Width	34 mm
		Thickness	0.04 mm
Cathode	LSCF + GDC	Density	6180 kg/m^3
		Specific heat	600 J/(kg·K)
		Thermal conductivity	9.6 W/(m·K)
		Tortuosity	3
		Porosity	0.3
		Permeability	1×10^{-12}
		Electrical conductivity	7937 S/m
		Length	100 mm
		Width	34 mm
		Thickness	0.56 mm
Electrolyte	8YSZ	Density	5900 kg/m^3
		Specific heat	410 J/(kg·K)
		Thermal conductivity	6.23 W/(m·K)
		Length	100 mm
		Width	34 mm
		Thickness	0.02 mm
Current collector	Steel	Density	7700 kg/m^3
		Specific heat	650 J/(kg·K)
		Thermal conductivity	25 W/(m·K)
		Electrical conductivity	1.5×10^7 S/m
		Length	100 mm
		Width	1 mm
		Height	1.6 mm
		Collector surface	Length 100 mm, Width 34 mm
		Rib size between channels	Length 100 mm, Width 1 mm, Height 1.6 mm
		Dimensions of one fuel/air channel	Length 100 mm, Width 1.4 mm, Height 1.4 mm

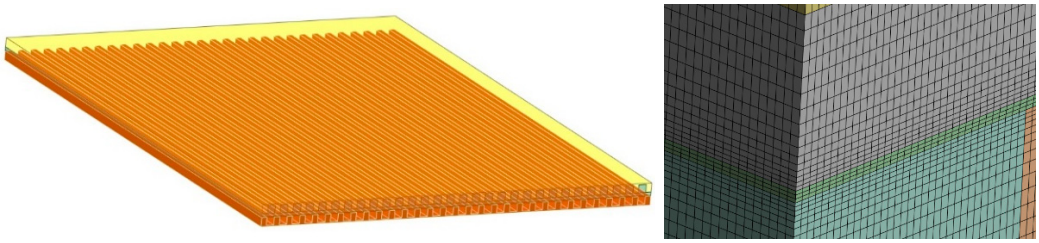

(**a**) (**b**)

Figure 1. (**a**) Three-dimensional model of a 30-channel planar SOFC; (**b**) fragment of a grid with condensation for a 3D model of an SOFC cell. Cell operating parameters are presented in Table 1.

2.1. Model Assumptions and Simplifications

The inlet pressure is atmospheric; the flow is laminar; for carbon-containing fuels, only steam reforming and carbon dioxide conversion are allowed; the operating temperature range is 700–1000 °C; perfect seal; there is no leakage effect; heat loss to the environment is based only on radiation; Joule heating is neglected in the model; work in a stationary mode; chemical reactions occur in one stage.

The processes in the cell are a combination of substance transfer, heat exchange, electron transfer, and electrochemical reactions.

The distribution of velocities and pressures in each cell, independent of time and space, is determined using the momentum conservation equations (Navier–Stokes equations). The processes of diffusion of chemical substances in laminar flow are described by Fick's law.

When modeling gas flows in fluid zones, the laws of the conservation of mass, momentum, and energy of incompressible laminar flows are applied. For a finite volume dV, the fundamental equations are applied under stationary conditions $\partial/\partial t = 0$.

In the case of carbon-containing fuels such as synthesis gas containing methane or carbon monoxide, the forward electrochemical conversion rate of CH_4 is quite low. A rapid vapor shift reaction is also observed at the SOFC operating temperature to form CO/H_2 and CO_2/H_2O, which reach equilibrium almost instantly. Thus, the electrochemical conversion of CO is indirectly modeled by the additional electrochemical conversion of hydrogen and includes the rate of the carbon monoxide conversion reaction.

The steam-reforming reaction of methane is endothermic, and the electrochemical oxidation of hydrogen is an exothermic reaction. This results in a temperature gradient within the stack. Therefore, the model must include the corresponding homogeneous gas methane steam reforming and steam shift reactions.

In this work, a numerical model was developed based on the commercial software package Ansys Fluent. The model simultaneously took into account thermophysical and electrochemical effects to study the performance of SOFC operating on reformed synthesis gas. The reactions of the steam reforming of methane, steam reforming of carbon monoxide, and electrochemical reactions in the porous anode were also taken into account.

2.2. Mathematical Equations

For all chemical substances, mass is stored in liquid regions, and the composition changes due to electrochemical reactions.

$$m_{i,in} + \sum\nolimits_k c_{i,\,k} v_k = m_{i,out} \tag{1}$$

where $m_{i,in}$—inlet mass flow of substances, kg/m^3·s;

$c_{i,\,k}$—stoichiometric coefficient of component i in reaction k;
v_k—reaction k rate.

Mass Conservation Equation

$$\nabla(\varepsilon\rho\vartheta) = m \tag{2}$$

where ε—porosity;

∇—the Nabla operator;
ϑ—velocity, m/s;
m—mass of the substance, kg/s;
ρ—density, kg/m^3.

The total consumption of substances consists of

$$m = m_{H_2} + m_{O_2} + m_{H_2O} \tag{3}$$

where the flow rate of each component (i) is calculated as follows

$$m_i = -\left(\frac{J_a}{2F}\right) M_i \tag{4}$$

where M_i—molar mass;

J_a—current density at the anode.

Due to the low Reynolds number and steady state, the conservation equation can be written as:

$$\nabla(\varepsilon\rho\vartheta\vartheta) = -\varepsilon\nabla\rho + \nabla\left[\varepsilon\mu\left(\nabla\vartheta + \left(\nabla\vartheta\right)^T\right)\right] + \frac{\mu\varepsilon^2}{k_g}\vartheta \quad (5)$$

k_g—gas phase permeability, m^2;
M—gas viscosity, kg/m·s.

The equation for the transfer of substances inside SOFC has the following form

$$\nabla\left(-\rho y_i \sum_{j\neq i}^{n} D_{eff,\,ij}\nabla x_j + \rho\vartheta y_i\right) = m_i \quad (6)$$

where y_i—mass fraction of the substance;

$D_{eff,\,ij}$—effective diffusion coefficient between substances i and j, m^2/s;
x_j—mole fraction of substance j.

The energy conservation equation will take the form:

$$\nabla(\varepsilon\rho c_p\vartheta T) = \nabla\left(k_{eff}\nabla T\right) + Q_v \quad (7)$$

where c_p—specific heat capacity, J/kg·K;

k_{eff}—thermal conductivity coefficient, W/m·K;
Q_v—heat flow, W/m^3.

The transfer of both electrons and ions contributes to the electrical balance calculation. The electronic charge arises in the electrodes and connections, while the ionic charge is present only in the electrodes and the electrolyte melt.

According to Ohm's law, the electronic charge balance is calculated as follows:
At the anode side:

$$\nabla(\sigma_a\nabla\varnothing_e) = -J_a A_V \quad (8)$$

At the cathode side:

$$\nabla(\sigma_c\nabla\varnothing_e) = -J_c A_V \quad (9)$$

According to Ohm's law, the ionic charge balance is calculated as follows:
In electrolyte:

$$\nabla(\sigma_{el}\nabla\varnothing_i) = 0 \quad (10)$$

At the anode side:

$$\nabla(\sigma_a\nabla\varnothing_i) = J_a A_V \quad (11)$$

At the cathode side:

$$\nabla(\sigma_c\nabla\varnothing_i) = J_c A_V \quad (12)$$

where ∅—exchange potential, i—ionic, e—electronic, el—electrolyte, V;

σ_a and σ_c—electrical conductivity of the anode and cathode, respectively, S/m;
J_a and J_c—volumetric current densities of the anode and cathode, respectively, A/m^2;
A_V—reaction area per unit volume, m^2/m^3.

The cell voltage is calculated from the following equation

$$V_{\text{яч}} = \mathrm{E}_N - \eta_{Ohm} - \eta_{act} - \eta_{conc} \quad (13)$$

where E_N—Nernst voltage (open circuit voltage), V;

η_{Ohm}, η_{act}, η_{conc}—ohmic, activation, and concentration overvoltage, respectively

The value of the Nernst voltage is related to the gas composition, operating pressure, operating temperature, etc., and is determined using the following equation

$$E_N = -\frac{\Delta G}{2F} + \frac{RT}{2F}\ln\left(\frac{P_{H_2} \times P_{O_2}^{0.5}}{P_{H_2O}}\right) \quad (14)$$

where T is temperature, K;

P—pressure, Pa;
R—gas constant, J/mol·K;
F—Faraday constant, Cul/mol;
ΔG—Gibbs energy, J.

Activation voltage loss is calculated using the Butler–Volmer equation

$$J = J_0\left\{exp\left(\frac{azF_{act}}{RT}\right) - exp\left[-\frac{(1-a)zF_{act}}{RT}\right]\right\} \quad (15)$$

where J—current density at the electrodes, A/m^2;

a—charge transfer coefficient;
J_0—represents the exchange current density, A/m^2;
z—electrons number.

It is difficult to directly calculate the activation voltage loss according to the Butler–Volmer equation in most cases. At high-activation polarization, the second term in the Butler–Volmer equation will be much smaller compared to the first term and can be eliminated. The resulting expression is the Tafel expression

$$\eta_{act} = \frac{RT}{azF} ln\left(\frac{j}{j_0}\right) \quad (16)$$

At low-activation polarization, the well-known linear current potential relation is obtained

$$\eta_{act} = \frac{RT}{zFj_0} j \quad (17)$$

Concentration polarization occurs when the fuel is consumed at the electrode–electrolyte interface, and the gas concentration decreases at the reaction sites. Concentration polarization becomes a significant loss at high current densities and low concentrations. The main factors contributing to concentration polarization are the diffusion of gases through a porous medium and the dissolution of reactants and products. For typical SOFC operating conditions, diffusive transport will dominate, and convective transport can be neglected. Molecular diffusion and Knudsen diffusion describe diffusive transport through a porous electrode. Their contribution to diffusive transport is closely related to the microphysical characteristics of the porous material (i.e., porosity, tortuosity, pore size, and permeability).

The concentration voltage loss is expressed as the following equation

$$\eta_{conc} = -\frac{RT}{zF} ln\left(\frac{y_{H_2} \cdot X_{H_2O}}{y_{H_2O} \cdot X_{H_2}}\right) \quad (18)$$

where X—concentration at the inlet, y—concentration at the outlet.

Ohmic polarization occurs in the electrode materials (anode and cathode), interconnections, and electrolytes. These losses represent the resistance to the flow of electrons in the electrodes and ions in the electrolyte.

Ohmic voltage losses are described as follows:

$$\eta_{Ohm} = R_{Ohm} \times j \quad (19)$$

It is possible to model these losses over a wide temperature range using the Arrhenius equation

$$R_{Ohm}(T) = \frac{T}{B_{Ohm}} exp\left(\frac{E_{act}}{RT}\right) \quad (20)$$

where B_{Ohm}—electrical materials conductivity depending on temperature, S·K/m^2;

E_{act}—activation energy, kJ/mol.

In the case of carbon-containing fuels such as synthesis gas containing methane or carbon monoxide, there is a fairly low forward electrochemical conversion rate of CH_4 and a rapid vapor shift reaction in the SOFC operating temperature to form CO/H_2 and CO_2/H_2O, which reach equilibrium almost instantly. Thus, the electrochemical conversion of CO is indirectly modelled through the additional electrochemical conversion of hydrogen and includes the rate of the carbon monoxide conversion reaction.

Since the methane steam reforming reaction is endothermic and the electrochemical oxidation of hydrogen is an exothermic reaction, it is the main cause of the temperature gradient within the stack. The model must include the corresponding homogeneous gas methane steam reforming reactions and the steam shift reaction. The steam reforming reaction is implemented as a direct volumetric gas reaction with a reaction rate of ϑCH_4.

$$\vartheta = k \times p_{CH_4}^m \times p_{H_2O}^n \times exp\left(-\frac{E_{act}}{RT}\right) \quad (21)$$

where k—reaction rate constant;

m, n—experimental reaction orders for substances

The steam shift reaction rate ϑCO can be calculated as follows [31]:

$$\vartheta = k_1\left(p_{H_2O}p_{CO} - \frac{p_{H_2}p_{CO_2}}{k_2}\right) \quad (22)$$

$$k_1 = Aexp\left(-\frac{E_{act}}{RT}\right) \quad (23)$$

where A—experimental pre-exponential factor;

k_1—forward reaction rate constant;
k_2—reverse reaction rate constant.

The Nernst potential in a gas mixture of equilibrium composition is equivalent for each oxidation reaction considered.

$$V_N = -\frac{\Delta^R G(T, p_0, \{p_i\})}{n^{el}F} = \frac{RT}{4F}\ln\left(\frac{p_{O_2}^{anode}}{p_{O_2}^{cathode}}\right) \quad (24)$$

As a consequence, the hydrogen oxidation reaction provides the same Nernst voltage as the oxidation of carbon monoxide in a gas mixture at equilibrium.

$$V_N = -\frac{\Delta^R G_0^{H_2}(T)}{z_{H_2}^{el}F} = -\frac{RT}{z_{H_2}^{el}F}\ln\left(\frac{p_{H_2O}\cdot p_0^{0.5}}{p_{H_2}\cdot p_{O_2}^{0.5}}\right) \quad (25)$$

$$V_N = -\frac{\Delta^R G(T, p_0, \{p_i\})}{z_{CO}^{el}F} = -\frac{RT}{z_{CO}^{el}F}\ln\left(\frac{p_{CO_2}\cdot p_0^{0.5}}{p_{CO}\cdot p_{O_2}^{0.5}}\right) \quad (26)$$

3. Results

The current density versus voltage dependence of the numerical model showed acceptable accuracy with the data obtained from the manufacturer, as shown in Figure 2. The correlation coefficient is 0.998.

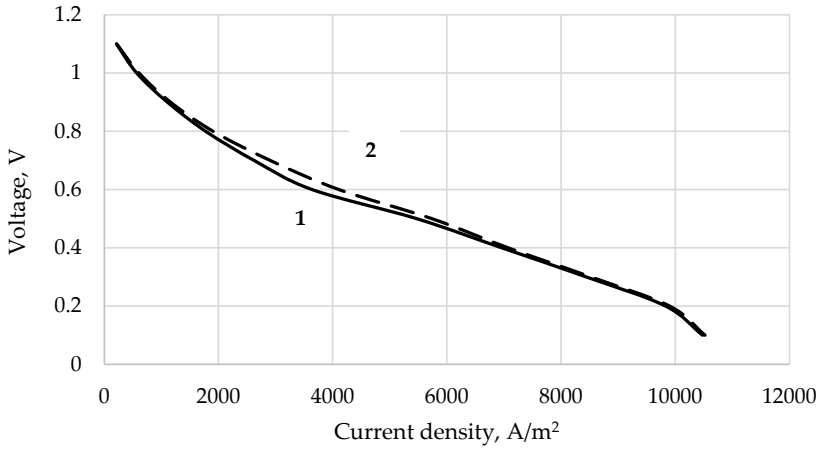

Figure 2. Current–voltage characteristics for hydrogen fuel based on the results of experimental data and numerical simulation. 1—Results from the experimental model. 2—Digital model results.

The results of the numerical modeling of electrochemical and heat-mass transfer processes in SOFCs make it possible to predict the influence of initial parameters, such as fuel composition, consumption, and the temperature of the fuel, air, and water (steam) on technical characteristics for more efficient electricity generation. Hydrogen was considered as the reference fuel for the fuel cell. Methane is also the base fuel for high-temperature solid oxide fuel cells due to its ability to reform within the fuel cell. The synthesis gas used for calculations is a product of reformed fuel gas from oil refineries after desulfurization. The composition of the synthesis gas is presented in Table 2.

For three types of fuel (hydrogen, methane, synthesis gas), current–voltage and watt–ampere characteristics were obtained (Figure 3).

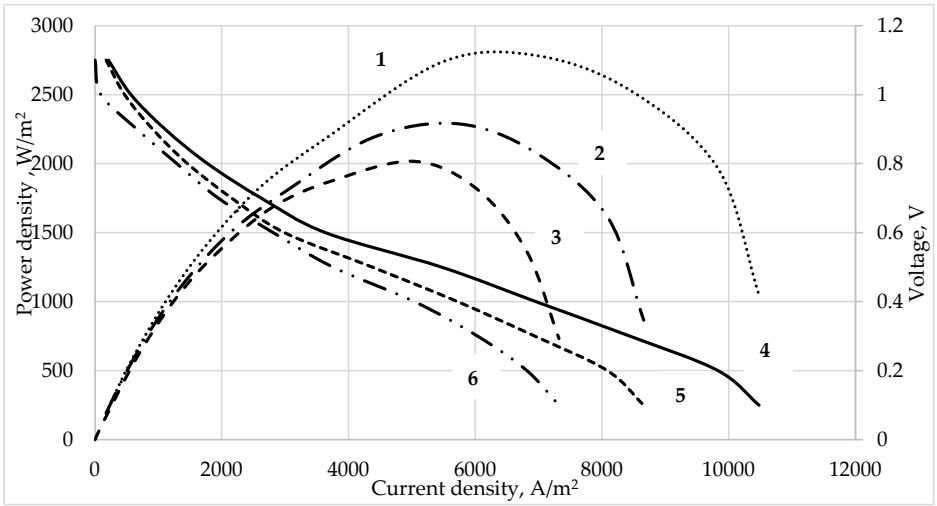

Figure 3. Current–voltage and watt–ampere curves of various SOFC fuels. Power density: hydrogen—1, methane—2, synthesis gas—3. Current density: hydrogen—4, methane—5, synthesis gas—6.

The maximum power density can be obtained when operating on hydrogen fuel. Synthesis gas contains a large amount of hydrogen in its composition and shows a high power density comparable to methane.

An analysis of the thermodynamic and electrical characteristics of SOFC operation on synthesis gas in comparison with hydrogen fuel, as a reference, was carried out. To simulate the SOFC operation in various modes, characteristics such as cell voltage, reagent supply rate, and fuel and air inlet temperatures were sequentially changed.

3.1. The Influence of the Supplied Reagents Temperature on the Electrical Characteristics of the Fuel Cell

As the temperature at the anode and cathode input increases, the current density increases linearly (Figure 4). This is due to the fact that high temperature facilitates the steam-reforming reaction of methane and increases the molar fractions of H_2 and CO (Figure 5). It must be emphasized that hydrogen and carbon monoxide are the main reagents that produce electric current.

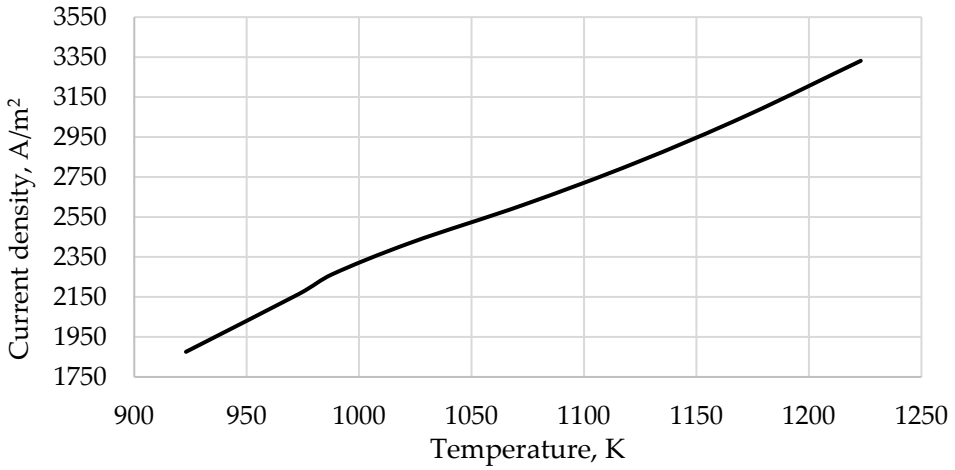

Figure 4. Dependence of the change in current density on temperature when operating on synthesis gas.

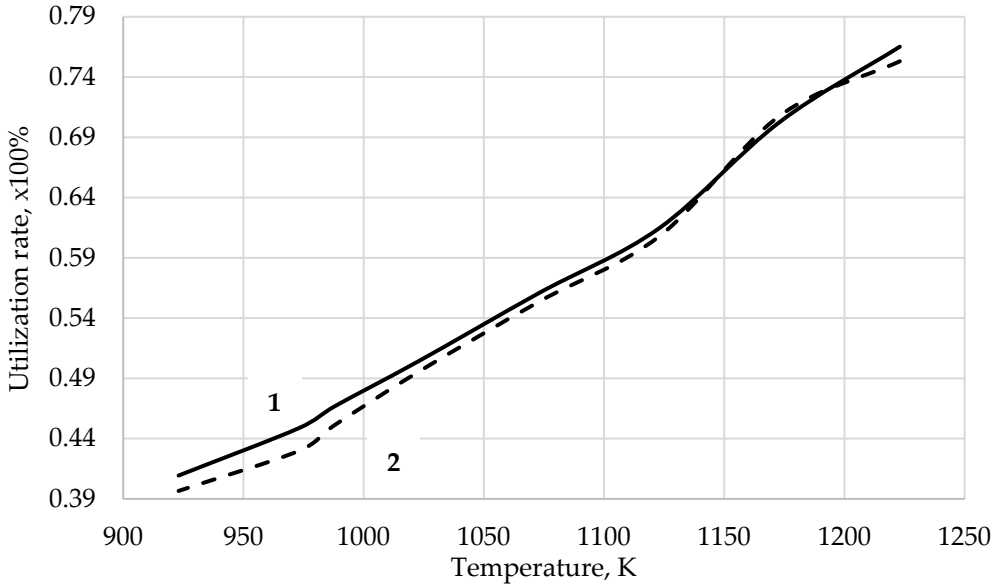

Figure 5. Dependence of changes in reagent utilization on temperature changes when operating on synthesis gas. Hydrogen utilization rate—1. Carbon monoxide utilization rate—2.

3.2. The Influence of Voltage Applied to the Cell on the Thermodynamic Characteristics of SOFC

As the voltage decreases, the temperature at the anode and cathode outlet and the maximum temperature gradient increase for both synthesis gas (Figure 6) and hydrogen (Figure 7). It should be noted that the operating temperatures of the fuel cell are in the range of 900–1300 K. At the same time, it is undesirable to allow a high-temperature rise due to the possible degradation of the fuel cell. Therefore, determining the operating voltage based on a numerical simulation in which the temperature will not exceed permissible limits is a primary task.

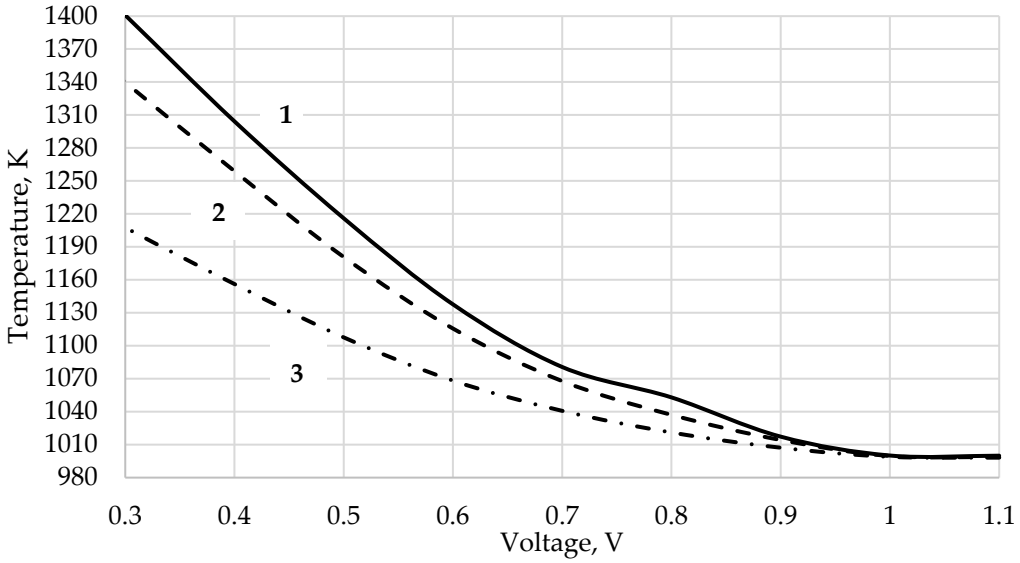

Figure 6. Dependence of temperature change on voltage when operating on synthesis gas. Maximum temperature—1, cathode outlet temperature—2, anode outlet temperature—3.

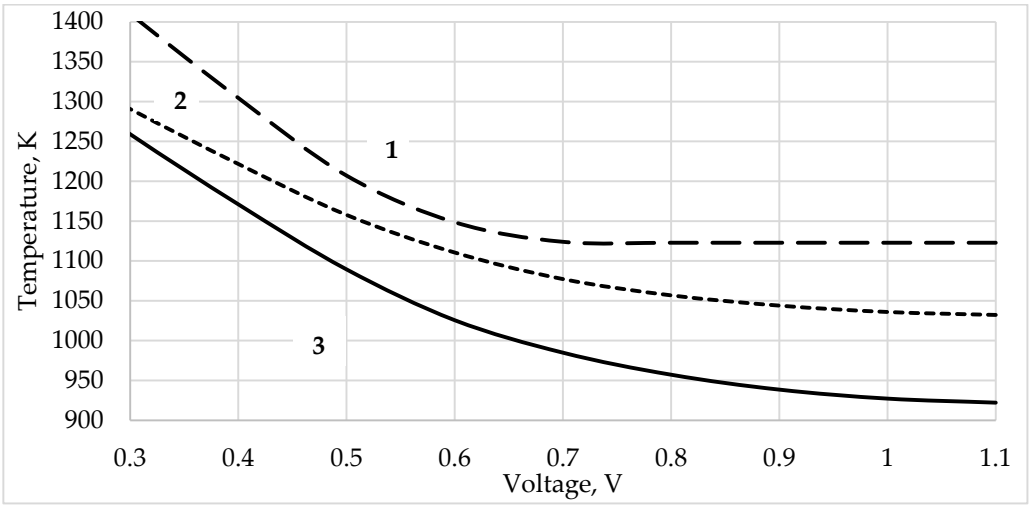

Figure 7. Dependence of temperature change on voltage when operating on hydrogen fuel. Maximum temperature—1, cathode outlet temperature—2, anode outlet temperature—3.

The inflection of the curves is noted at a voltage of 0.6–0.7 V. At this voltage, the temperature difference for the synthesis gas is 70 K from the anode outlet and 117 K from the cathode outlet. When operating on hydrogen, the temperature difference is 27 K from the anode outlet and 112 K from the cathode outlet. The maximum temperature gradient at these voltages for synthesis gas is 139 K; for hydrogen, it is 150 K. This is due to the thermodynamic features of the reactions. The reactions of hydrogen oxidation and steam reforming of carbon dioxide are exothermic. Steam methane reforming is an endothermic reaction. Therefore, the observed temperature gradient is lower for synthesis gas than for hydrogen fuel. The temperature gradient magnitude is important in understanding the amount of useful heat, which can be produced using SOFC operations. Useful heat is a product of a fuel cell, which can be used for heating needs when operating in the mini-thermal power station mode.

The temperature distribution during SOFC operation along the cell for synthesis gas and hydrogen is shown in Figure 8a,b, respectively. It can be noted that if synthesis gas is used as a fuel, several simultaneous reactions with multidirectional thermal effects occur and the temperature distribution along the cell is complex (Figure 8a). When pure hydrogen

is supplied, a rise in temperature is observed almost immediately after the fuel enters the cell (Figure 8a).

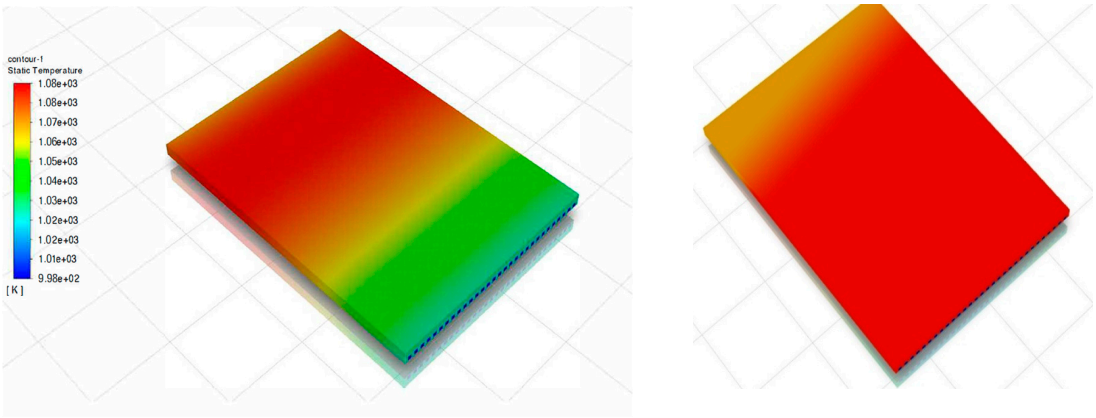

(**a**) (**b**)

Figure 8. Temperature distribution for synthesis gas (**a**); for hydrogen fuel (**b**) at 0.6 V. The input temperature is 998 K.

3.3. The Influence of Fuel Supply Rate on the Electrical and Thermodynamic Characteristics of SOFC

The rate of the reagent supply has a significant impact on the operating parameters of the electrochemical cell. Thus, with a decrease in airflow, an increase in the outlet temperature from the anode and cathode, as well as the maximum temperature difference across the cell, is observed (Figure 9). This is because insufficient air supply can lead to a high-temperature gradient. Therefore, the ratio of air to fuel must be selected in such a way as not to cause thermal stresses along the cell, while ensuring a sufficient oxygen utilization rate. According to the calculation results, the optimal molar ratio of air and fuel for synthesis gas was 6.74.

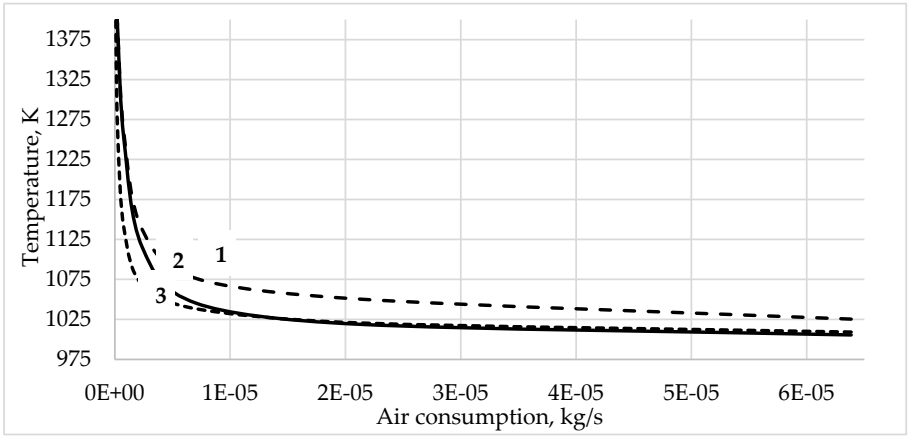

Figure 9. Dependence of the outlet temperature of gases and the temperature gradient along the cell on the flow rate of air supplied to the cathode. Maximum temperature—1, cathode outlet temperature—2, anode outlet temperature—3.

In contrast to SOFC operating on hydrogen (Figure 10), this study shows that the reagent utilization coefficient decreases slightly with an increasing synthesis gas supply rate (Figures 11 and 12). This is due to the fact that high gas velocity inhibits the increase in the molar fractions of H_2 and CO in the steam methane reforming reaction according to Le Chatelier's principle. For SOFCs running on hydrogen, a high gas supply rate makes it possible to maintain a high molar fraction of the fuel, which would otherwise decrease along the channel due to the electrochemical reaction.

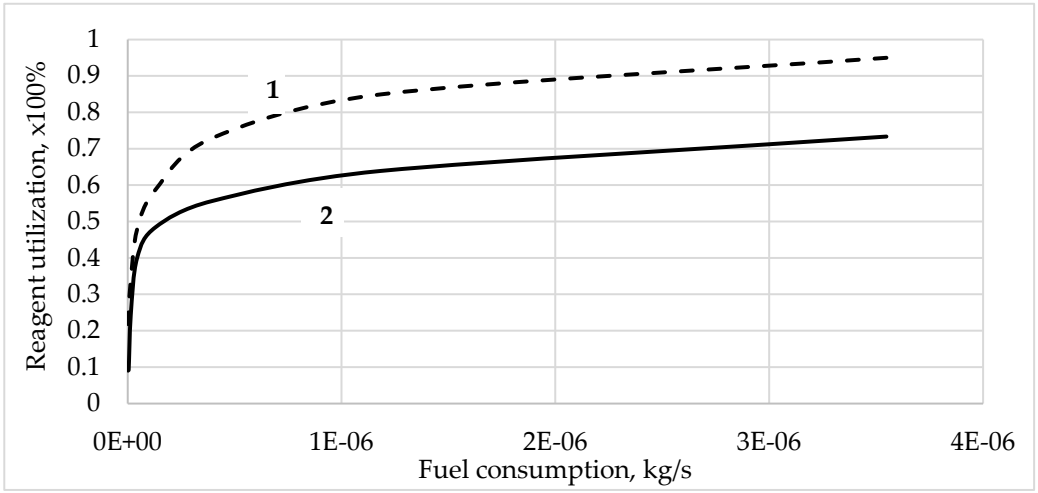

Figure 10. Dependence of changes in reagent utilization when operating on hydrogen fuel on the feed rate. Fuel utilization—1. Air utilization—2.

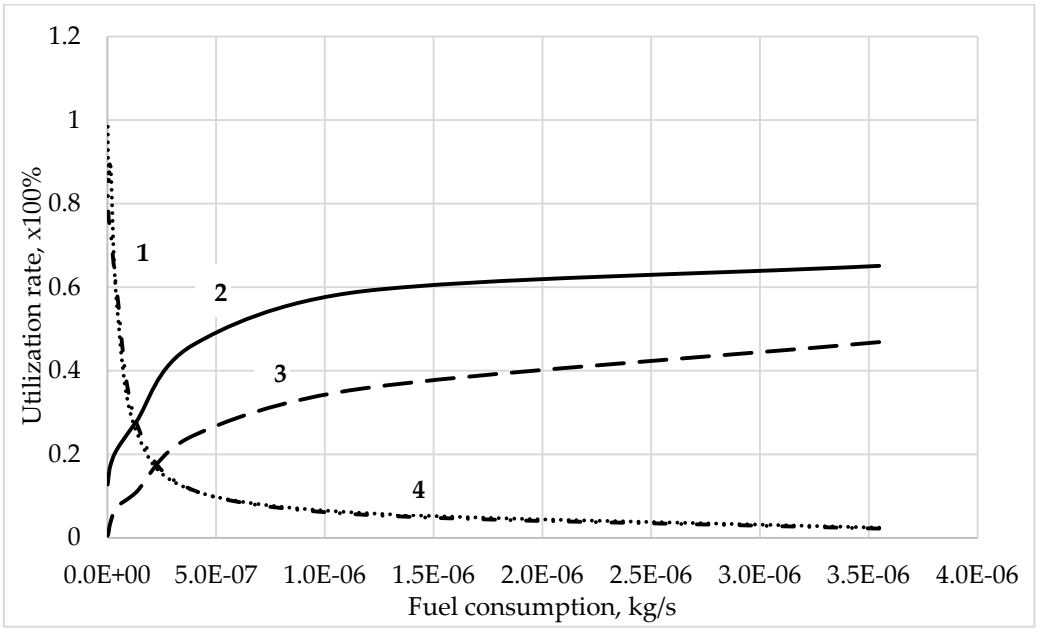

Figure 11. Dependence of changes in reagent utilization when operating on synthesis gas on the fuel supply rate. Hydrogen utilization rate—1, methane utilization rate—2, oxygen utilization rate—3, carbon monoxide utilization rate—4.

Thus, high gas velocity makes it possible to achieve high electrical power for SOFCs when operating on hydrogen but slightly reduces the electrical power of SOFCs when operating on hydrocarbon fuels. However, as fuel consumption increases, the current density increases. The increase in current density when operating on hydrogen is greater than for synthesis gas (Figure 13).

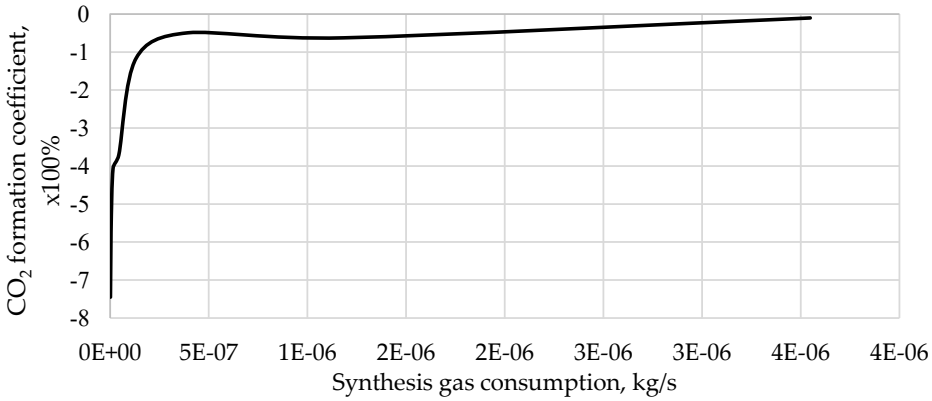

Figure 12. Dependence of changes in carbon dioxide formation when operating on synthesis gas on the fuel supply rate.

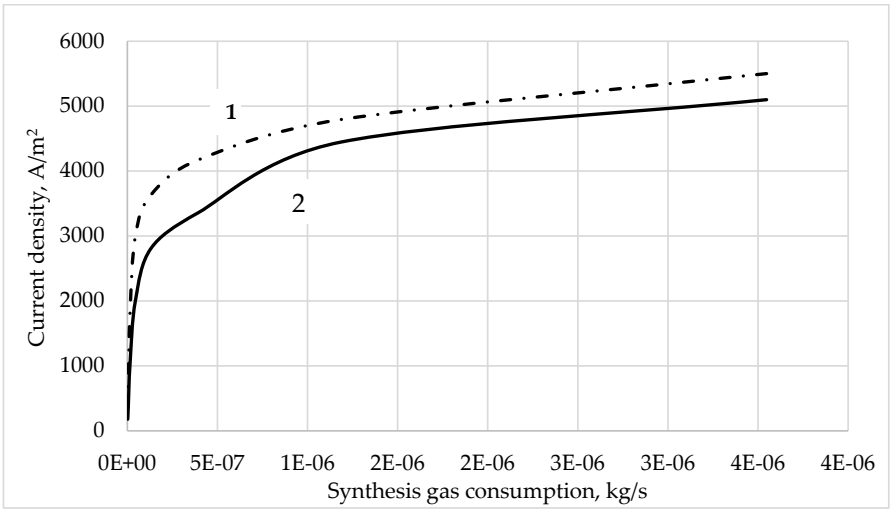

Figure 13. Dependence of changes in SOFC current density on different types of fuel on consumption. Hydrogen—1, synthesis gas—2.

As the reagent utilization rate increases, the current density and specific power increase (Figure 14). For synthesis gas, the maximum power density is achieved with a utilization coefficient of hydrogen—0.43, methane—0.36, carbon monoxide—0.4, and oxygen—0.11.

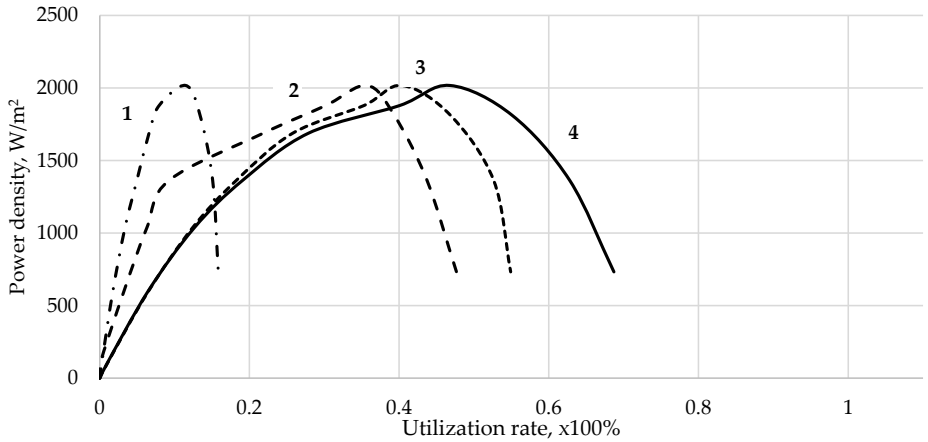

Figure 14. Dependence of the change in power density on the utilization of reagents in the synthesis gas supplied to the SOFC. Oxygen utilization rate—1, methane utilization rate—2, carbon monoxide utilization rate—3, hydrogen utilization rate—4.

The distribution of reagents along the cell when synthesis gas is supplied at a voltage of 0.6 V is shown in Figures 15–21.

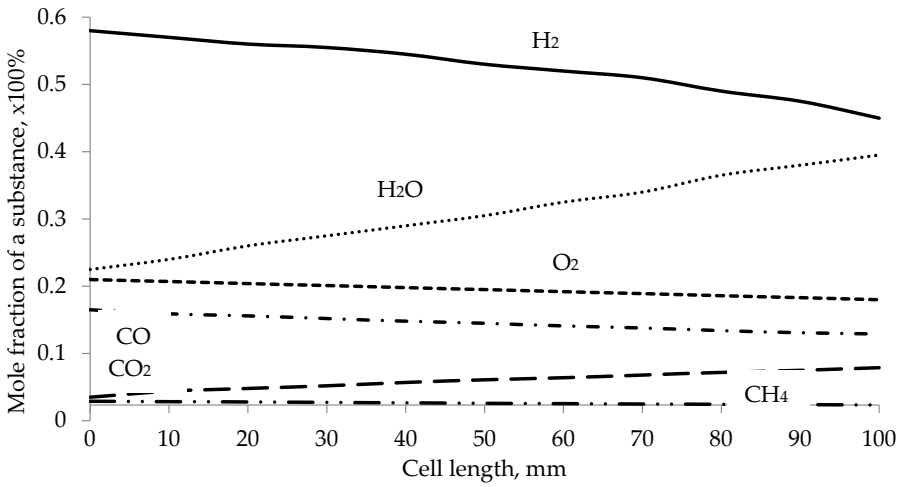

Figure 15. Distribution of reagents along the channels of the cell when operating on synthesis gas.

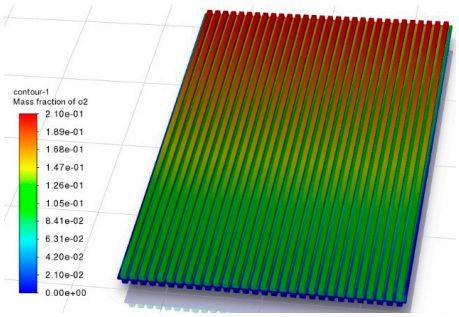

Figure 16. Oxygen distribution along the cathode channels.

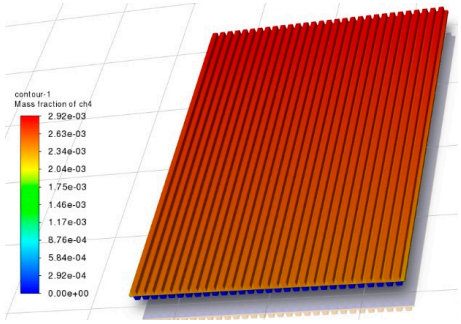

Figure 17. Distribution of CH_4 along the channels and anode electrode.

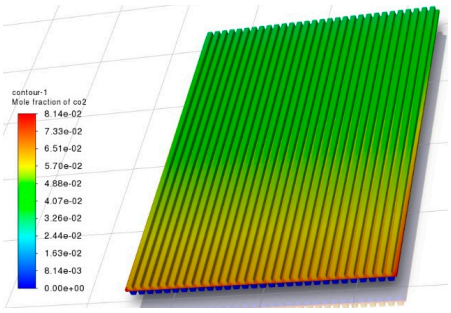

Figure 18. CO_2 formation in the channels of the anode part.

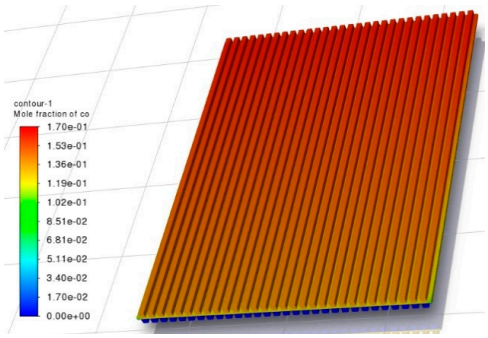

Figure 19. Distribution of CO across the channels and anode electrode.

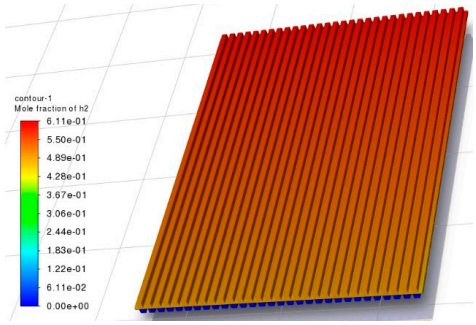

Figure 20. Distribution of H_2 along the channels and anode electrode.

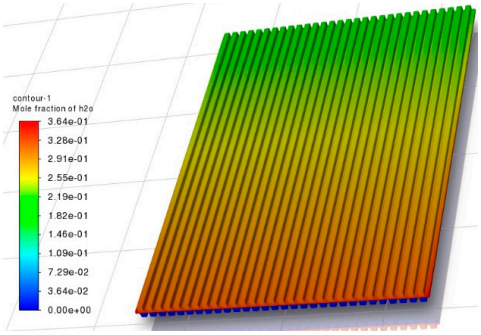

Figure 21. Formation of H_2O vapor in the channels and anode electrode.

Mass transfer in the fuel cell channels is presented in Figures 16–21. The current density distribution along the cell is shown in Figure 22.

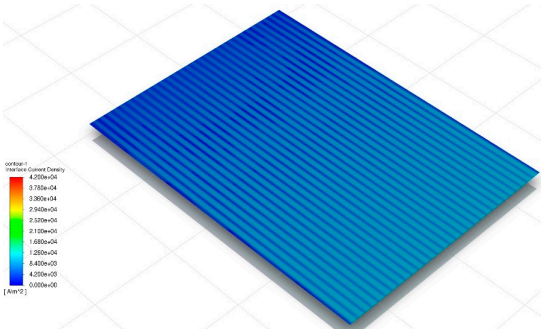

Figure 22. Current density distribution along the cell.

When synthesis gas is used as a fuel, steam reforming, carbon monoxide oxidation, and hydrogen–oxygen reactions occur simultaneously. The red color in Figures 16–21 denotes a high content of the substance; by contrast, green denotes low content. Methane and oxygen

(Figures 16 and 17) are the main active reagents and enter the fuel cell, where they are consumed to produce hydrogen, CO, CO_2, and water. Moreover, methane is not completely consumed and partially remains in the outlet gas mixture. Hydrogen is supplied to the fuel mixture in fairly large quantities and is also formed in the steam reforming reaction. Therefore, it is present in large quantities until the middle of the channel, and then it begins to be consumed in the electrochemical reaction (Figure 20). Carbon monoxide also enters the fuel mixture and reacts with oxygen to form carbon dioxide (Figure 19). Carbon dioxide is practically absent from the initial fuel mixture but is formed in significant quantities as a result of methane steam reforming reactions and the oxidation of carbon monoxide (Figure 18). The presence of water at the fuel cell inlet is necessary for the methane steam reforming reaction to occur. Therefore, it is consumed as the gas mixture moves in the fuel cell. At the same time, the resulting hydrogen reacts with oxygen to form water. The combination of these processes leads to a slight increase in the yield of water vapor from the fuel cell (Figure 21). Thus, simultaneously occurring chemical reactions lead to the emergence of an electric current with an increase in charge density from input to outlet and the dark blue color changes to light blue (Figure 22).

The fuel utilization rate is one of the main factors affecting the dynamic performance and service life of SOFC. The electrical efficiency of the cell is increased by more than 25% by changing fuel consumption from 40% to 90%. Such sharp changes are associated with the strong dependence of efficiency and fuel utilization on the inlet fuel flow rate. It can be seen that increasing fuel use significantly affects the efficiency of fuel cells (Figure 23). However, in practice, fuel cells operating at high fuel utilization rates (>95%) suffer from rapid reductions in current density and efficiency [40]. Therefore, despite the increase in efficiency, the fuel utilization rate should be maintained within an acceptable range from 0.7 to 0.9 to prevent fuel depletion, sudden voltage rise, and associated irreversible damage, as recommended by manufacturers [41].

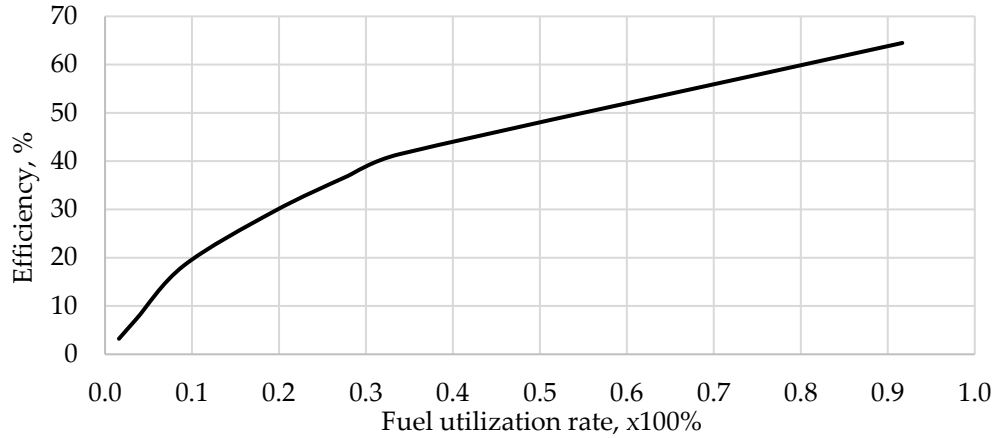

Figure 23. Dependence of electrical efficiency on fuel utilization rate.

The results of SOFC operation on various types of fuel, obtained using a numerical simulation, are summarized in Table 3.

The results of the study show that the highest electrical efficiency can be obtained when operating SOFCs on hydrogen. Synthesis gas from industrial waste obtained through reforming also shows good results in terms of productivity, fuel consumption, and reagent utilization rate due to its high content of hydrogen, methane, and carbon monoxide. The steam-to-methane ratio is 2.5 and is within the range (2.0–3.0) reported in the literature at which carbon deposition does not occur. In the case of using synthesis gas, additional water is formed in the reaction of hydrogen with oxygen, which can also be spent on methane reforming. Therefore, the required steam-to-methane ratio is less, specifically, 2.0.

Table 3. Calculated efficiency parameters for SOFC operation on various types of fuel.

Parameter	Hydrogen	Methane	Synthesis Gas
Electrical efficiency,%	64.2	55	49.8
Fuel consumption per 1 W, mol/h	0.0003	0.024	0.03
Molar ratio of water and fuel	-	2.5	2
Air to fuel mole ratio	1.24	10	6.74
Reagent utilization rate	0.66 H_2 0.68 O_2	0.71 CH_4 0.3 O_2	0.36 CH_4 0.4 CO 0.43 H_2 0.11 O_2
Temperature gradient in the channel, K (at 0.6 V)	150	131	139
Temperature gradient at the anode outlet, K (at 0.6 V)	27	56	70
Temperature gradient at the cathode outlet, K (at 0.6 V)	112	115	117
Thermal power, W	98.7	68.5	54.6
Net calorific value of fuel, MJ/kg	120.9	50	46

The heat generated by the fuel cell can be used to carry out a pre-reforming reaction or to hybridize the cycle with other power units. The maximum temperature gradient can be obtained at the outlet of cathode gases when operating on synthesis gas. However, the total thermal power of the cell is higher for hydrogen fuel because its calorific value exceeds that of other fuels. The temperature difference along the channel is also highest for hydrogen fuel and is intermediate for synthesis gas. High-temperature differences along the channel increase equipment degradation.

4. Conclusions

A digital model of a high-temperature solid oxide fuel cell has been developed based on the commercial Ansys Fluent 2020 R2 software package. The developed model allows for the simultaneous calculation of hydrodynamic, electrochemical, and heat and mass transfer processes in a fuel cell.

The calculation results were verified using the developed digital model with the performance characteristics of a real solid oxide fuel cell. According to the results of digital modeling, the predicted dependence of the current density on voltage for the constructed 3D model showed acceptable accuracy with data received from the manufacturer with a correlation coefficient of 0.998.

Using the method of numerical modeling of SOFC, the influence of changes in initial parameters, such as the composition of the fuel used, consumption and temperature of the fuel, air, and water (steam) on the outlet characteristics of the fuel cell for more efficient generation of electricity, was studied.

Fuel cell operating temperatures ranged from 900 to 1300 K. Such temperatures correspond to a cell operating voltage of 0.6–0.7 V for all types of fuel and are necessary to prevent fuel cell degradation. Chemical reaction thermodynamics allows one to obtain a thermal outlet power of the cell of nearly 98.7 W for hydrogen, 68.5 W for methane, and 54.6 W for synthesis gas. This thermal power can be used for heating needs when operating in the mini-CHPP mode.

Using mathematical modeling optimal flow rates of air and reagents were selected that do not cause temperature stress along the cell while ensuring a sufficient coefficient of fuel and oxygen utilization. Air must be supplied in some excess and be at a molar ratio of 1.24 when operating on hydrogen, 10 when operating on methane, and 6.74 when operating on synthesis gas. Fuel utilization coefficients (hydrogen, methane, and carbon monoxide) for all types of fuel are selected in such a way that the maximum specific power is achieved. At the same time, the fuel utilization rate should be maintained within an acceptable range

from 0.7 to 0.9 to prevent fuel depletion, sudden voltage rises, and associated irreversible damage, as recommended by manufacturers. The utilization rate of hydrogen is 0.66 in hydrogen fuel, methane 0.71 in natural gas, and the main combustible reagents in synthesis gas are methane, CO, and hydrogen—0.36, 0.4, and 0.43, respectively.

The molar ratio of water is also important for ensuring the kinetics and thermodynamics of chemical reactions and, according to the calculations performed, corresponds to practical results: 2.5 for methane and 2.0 for synthesis gas.

The obtained results make it possible to achieve an electrical efficiency of the fuel cell, which is 64.2% for hydrogen fuel, 55% for methane, and 49.8% for synthesis gas.

The effectiveness of the proposed digital model has been proven. The developed model expands the possibilities of creating a decarbonized process for producing energy from hydrogen-containing gas waste from deep oil refining for utilization in a high-temperature fuel cell.

It was demonstrated that, for social facilities and small industries, such technology can be an effective solution for obtaining electrical power of no more than 100 kW. A high-temperature fuel cell can provide consumers with heat and electricity, as well as the industrial sector with high-tech heat and steam when operating in the mini-CHPP mode.

Author Contributions: A.A.C. and A.A.F. worked on all the tasks, A.A.F. and N.D.C. worked on the literature review, I.K.I. and A.A.F. conducted computational studies, I.K.I. and P.G.K. performed the supervision, and all authors analyzed the results. All authors have read and agreed to the published version of the manuscript.

Funding: This study is financed by the European Union—NextGenerationEU—through the National Recovery and Resilience Plan of the Republic of Bulgaria, project N° BG-RRP-2.013-0001-C01. This research was also co-funded by the Ministry of Science and Higher Education of the Russian Federation "Study of processes in a fuel cell-gas turbine hybrid power plant" (project code: FZSW-2022-0001).

Data Availability Statement: The original contributions presented in the study are included in the article, further inquiries can be directed to the corresponding author.

Conflicts of Interest: The authors declare no conflicts of interest.

References

1. Iliev, I.; Filimonova, A.A.; Chichirov, A.A.; Chichirova, N.D.; Pechenkin, A.V.; Vinogradov, A. Theoretical and Experimental Studies of Combined Heat and Power Systems with SOFCs. *Energies* **2023**, *16*, 1898. [CrossRef]
2. Hussain, J.; Ali, R.; Akhtar, M.N.; Jaffery, M.H.; Shakir, I.; Raza, R. Modeling and simulation of planar SOFC to study the electrochemical properties. *Curr. Appl. Phys.* **2020**, *20*, 660–672. [CrossRef]
3. Andersson, M.; Yuan, J.; Sundén, B. SOFC modeling considering electrochemical reactions at the active three phase boundaries. *Int. J. Heat Mass Transf.* **2012**, *55*, 773–788. [CrossRef]
4. Ilbas, M.; Kumuk, B. Numerical modelling of a cathode-supported solid oxide fuel cell (SOFC) in comparison with an electrolyte-supported model. *J. Energy Inst.* **2019**, *92*, 682–692. [CrossRef]
5. İlbaş, M.; Kümük, B. Modeling and analysis of a model solid oxide fuel cell running on low calorific value coal gases. *Int. J. Hydrogen Energy* **2020**, *45*, 3577–3583. [CrossRef]
6. Amedi, H.R.; Bazooyar, B.; Pishvaie, M.R. Control of anode supported SOFCs (solid oxide fuel cells): Part I. mathematical modeling and state estimation within one cell. *Energy* **2015**, *90*, 605–621. [CrossRef]
7. Xia, B.; Sun, D.W. Applications of computational fluid dynamics (CFD) in the food industry: A review. *Comput. Electron. Agric.* **2002**, *34*, 5–24. [CrossRef]
8. Norton, T.; Sun, D.W. Computational fluid dynamics (CFD)—An effective and efficient design and analysis tool for the food industry: A review. *Trends Food Sci. Technol.* **2006**, *17*, 600–620. [CrossRef]
9. Yang, B.; Wang, J.; Zhang, M.; Shu, H.; Yu, T.; Zhang, X.; Yao, W.; Sun, L. A state-of-the-art survey of solid oxide fuel cell parameter identification: Modelling, methodology, and perspectives. *Energy Convers. Manag.* **2020**, *213*, 112856. [CrossRef]
10. Horr, S.; Mohcene, H.; Bouguettaia, H.; Moussa, H.B. Performance analysis of AS-SOFC fuel cell combining single and sinusoidal flow field: Numerical study Renew. *Energy Environ. Sustain.* **2021**, *6*, 18. [CrossRef]
11. Błesznowski, M.; Sikora, M.; Kupecki, J.; Makowski, Ł.; Orciuch, W. Mathematical approaches to modelling the mass transfer process in solid oxide fuel cell anode. *Energy* **2022**, *239*, 121878. [CrossRef]
12. Pongratz, G.; Subotić, V.; Hochenauer, C.; Scharler, R.; Anca-Couce, A. Solid oxide fuel cell operation with biomass gasification product gases: Performance- and carbon deposition risk evaluation via a CFD modelling approach. *Energy* **2022**, *244*, 123085. [CrossRef]

13. Ghorbani, B.; Vijayaraghavan, K. A review study on software-based modeling of hydrogen-fueled solid oxide fuel cells. *Int. J. Hydrogen Energy* **2007**, *44*, 13700–13727. [CrossRef]
14. Mehrabian, M.; Mahmoudimehr, J. A numerical study to determine proper steam-to-fuel ratio in a biogas-fueled solid oxide fuel cell for different levels of biogas methane content. *Proc. Inst. Mech. Eng. Part C J. Mech. Eng. Sci.* **2024**, *238*, 2439–2455. [CrossRef]
15. Machaj, K.; Kupecki, J.; Niemczyk, A.; Malecha, Z.; Brouwer, J.; Porwisiak, D. Numerical analysis of the relation between the porosity of the fuel electrode support and functional layer, and performance of solid oxide fuel cells using computational fluid dynamics. *Int. J. Hydrogen Energy* **2024**, *52*, 936–951. [CrossRef]
16. Li, Y.; Grimm, F.; Karl, J. Numerical and experimental analysis of the effects of tar components on single planar SOFC under high fuel utilization. *Electrochim. Acta* **2023**, *449*, 142234. [CrossRef]
17. Beloev, I.; Filimonova, A.; Pechenkin, A.; Gizzatullin, A.; Vinogradov, A.; Iliev, I. Numerical simulation of solid oxide fuel cell energy production processes. *Eng. Proc.* **2023**, *41*, 11. [CrossRef]
18. Zhao, C.; Yang, J.; Zhang, T.; Yan, D.; Pu, J.; Chi, B.; Li, J. Numerical modeling of manifold design and flow uniformity analysis of an external manifold solid oxide fuel cell stack. *Int. J. Hydrogen Energy* **2020**, *45*, 14440–14451. [CrossRef]
19. Kim, Y.J.; Jung, W.N.; Yu, J.H.; Kim, H.J.; Yun, K.S.; Kang, D.G.; Lee, M.C. Design and analysis of SOFC stack with different types of external manifolds. *Int. J. Hydrogen Energy* **2020**, *45*, 29143–29154. [CrossRef]
20. Zhang, X.; Espinoza, M.; Li, T.; Andersson, M. Parametric study for electrode microstructure influence on SOFC performance. *Int. J. Hydrogen Energy* **2021**, *46*, 37440–37459. [CrossRef]
21. Ren, J.; Wang, Y.; Shi, Y. Numerical simulation and thermal stress analysis of direct internal reforming SOFCs. *Int. J. Green Energy* **2022**, *19*, 399–409. [CrossRef]
22. Wang, C.; Yang, J.; Huang, W.; Zhang, T.; Yan, D.; Pu, J.; Chi, B.; Li, J. Numerical simulation and analysis of thermal stress distributions for a planar solid oxide fuel cell stack with external manifold structure. *Int. J. Hydrogen Energy* **2018**, *43*, 20900–20910. [CrossRef]
23. Sarmah, P.; Gogoi, T.K.; Das, R. Estimation of operating parameters of a SOFC integrated combined power cycle using differential evolution based inverse method. *Appl. Therm. Eng.* **2017**, *119*, 98–107. [CrossRef]
24. Chen, H.; Chang, S.; Hsu, M.; You, C. Experimental and numerical study of innovative plate heat exchanger design in simplified hot box of SOFC. *Int. J. Heat Mass Transf.* **2021**, *181*, 121880. [CrossRef]
25. Altindal, S.; Erol, E.; Gurel, B. Numerical analysis of the effects of interconnector design and operating parameters on solid oxide fuel cell performance. *Int. J. Hydrogen Energy* **2024**, *52*, 1475–1490. [CrossRef]
26. Xiong, X.; Liang, K.; Ma, G.; Ba, L. Three-dimensional multi-physics modelling and structural optimization of SOFC large-scale stack and stack tower. *Int. J. Hydrogen Energy* **2023**, *48*, 2742–2761. [CrossRef]
27. Kalra, P.; Garg, R.K.; Kumar, A. Parametric sensitivity analysis for a natural gas fueled high temperature tubular solid oxide fuel cell. *Heliyon* **2020**, *6*, e04450. [CrossRef] [PubMed]
28. Kim, D.H.; Bae, Y.; Lee, S.; Son, J.-W.; Shim, J.H.; Hong, J. Thermal analysis of a 1-kW hydrogen-fueled solid oxide fuel cell stack by three-dimensional numerical simulation. *Energy Convers. Manag.* **2020**, *222*, 113213. [CrossRef]
29. Li, P.; Chyu, M.K. Simulation of the chemical/electrochemical reactions and heat/mass transfer for a tubular SOFC in a stack. *J. Power Sources* **2003**, *124*, 487–498. [CrossRef]
30. Robinson, J.B.; Brown, L.D.; Jervis, R.; Taiwo, O.O.; Heenan, T.M.; Millichamp, J.; Mason, T.J.; Neville, T.P.; Clague, R.; Eastwood, D.S.; et al. Investigating the effect of thermal gradients on stress in solid oxide fuel cell anodes using combined synchrotron radiation and thermal imaging. *J. Power Sources* **2015**, *288*, 473–481. [CrossRef]
31. Beale, S.B.; Andersson, M.; Boigues-Muñoz, C.; Frandsen, H.L.; Lin, Z.; McPhail, S.J.; Ni, M.; Sundén, B.; Weber, A.; Weber, A.Z. Continuum scale modelling and complementary experimentation of solid oxide cells. *Prog. Energy Combust. Sci.* **2021**, *85*, 100902. [CrossRef]
32. Tikiz, I.; Taymaz, I.; Pehlivan, H. CFD modeling and experimental validation of cell performance in a 3-D planar SOFC. *Int. J. Hydrogen Energy* **2019**, *44*, 15441–15455. [CrossRef]
33. Zhang, Z.; Chen, J.; Yue, D.; Yang, G.; Ye, S.; He, C.; Wang, W.; Yuan, J.; Huang, N. Three-Dimensional CFD Modeling of Transport Phenomena in a Cross-Flow Anode-Supported Planar SOFC. *Energies* **2014**, *7*, 80–98. [CrossRef]
34. Hosseini, S.; Ahmed, K.; Tadé, M.O. CFD model of a methane fueled single cell SOFC stack for analyzing the combined effects of macro/micro structural parameters. *J. Power Sources* **2013**, *234*, 180–196. [CrossRef]
35. Faheem, H.H.; Abbas, S.Z.; Tabish, A.N.; Fan, L. A review on mathematical modeling of direct internal reforming- solid oxide fuel cells. *J. Power Sources* **2022**, *520*, 230857. [CrossRef]
36. Rossetti, I. Modeling of fuel cells and related energy conversion systems. *ChemEngineering* **2022**, *6*, 32. [CrossRef]
37. Reale, F.; Sannino, R. Numerical Modeling of Energy Systems Based on Micro Gas Turbine: A Review. *Energies* **2022**, *15*, 900. [CrossRef]
38. Omer, A.; Rahimipetroudi, I.; Rashid, K. Design and performance optimization of a direct ammonia planar solid oxide fuel cell for high electrical efficiency. *J. Power Sources* **2023**, *573*, 233135. [CrossRef]
39. Hollmann, J.; Fuchs, M.; Spiker, C.; Gardemann, U.; Steffen, M.; Luo, X.; Kabelac, S. System simulation and analysis of an lng-fueled SOFC system using additively manufactured high temperature heat exchangers. *Energies* **2022**, *15*, 941. [CrossRef]

40. Zhu, H.; Kee, R.J. Thermodynamics of SOFC efficiency and fuel utilization as functions of fuel mixtures and operating conditions. *J. Power Sources* **2006**, *161*, 957–964. [CrossRef]
41. Nayeripour, M.; Hoseintabar, M. A new control strategy of solid oxide fuel cell based on coordination between hydrogen fuel flow rate and utilization factor. *Renew. Sustain. Energy Rev.* **2013**, *27*, 505–514. [CrossRef]